DIRECT NUMERICAL SIMULATION OF NATURAL CONVECTION OVER HORIZONTAL PLATES

Daniele Venturi[1], Beatrice Pulvirenti[1], Sandro Salvigni[1]

[1]*DIENCA, Universita' degli Studi di Bologna, Viale Risorgimento 2, 40136 Bologna*
e-mail: daniele.venturi@mail.ing.unibo.it

ABSTRACT
Natural convective flows over horizontal plates in confined domains are investigated by direct numerical simulations. A wide range of Rayleigh numbers is considered, spanning steady laminar, unsteady periodic and chaotic transitional regime. The time dependent Boussinesq equations are discretized using a high order spectral/hp finite element method. The averaged Nusselt number turns out to be in very good agreement with the available experimental correlations. Transition form steady to unsteady laminar regime is observed in the range $Ra = 2.5 \div 3.5 \times 10^3$. The mechanism for heat transfer in proximity of the heated plate is investigated by the symmetric version of the proper orthogonal decomposition (POD) method.

Introduction

We consider the heat transfer and natural convective two dimensional flow over an isothermal upward-facing plate. Natural convective flows induced over horizontal and inclined heated plates have been the subjects of numerous investigations ([8; 7; 15; 6; 19; 18; 2; 10]) in recent decades. These flows are of interest in a number of engineering applications such as computer and electronic cooling, solar collection system and building energy system. We have performed accurate direct numerical simulations of the time dependent Boussinesq equations

$$\begin{cases} \frac{\partial \mathbf{u}}{\partial t} + (\mathbf{u}\cdot\nabla)\,\mathbf{u} = \frac{\mathrm{Gr}}{\mathrm{Re}^2}\theta\mathbf{j} - \nabla p + \frac{1}{\mathrm{Re}}\nabla^2\mathbf{u} \\ \frac{\partial \theta}{\partial t} + \mathbf{u}\cdot\nabla\theta = \frac{1}{\mathrm{RePr}}\nabla^2\theta \\ \nabla\cdot\mathbf{u} = 0 \end{cases} \tag{1}$$

at Rayleigh number ranging from $Ra = 10^2$ to $Ra = 4.75\times10^6$, using the high order spectral/*hp* finite element method described in [11]. The Prandt number is $Pr = 0.72$. Basic details on the numerical scheme used to couple the Navier-Stokes equation to the Fourier equation are given in the Appendix I. Other schemes similar to that proposed here has been proposed in [1] and [13]. In (1) $\mathbf{j}$ is the upward unit vector while $\mathbf{u}$ and θ are the dimensionless velocity and temperature fields respectively. The dimensionless temperature is defined by

$$\theta = \frac{T - T_\infty}{T_w - T_\infty} \tag{2}$$

where T_w is the uniform temperature at the plate surface and T_∞ is the reference temperature. Also,

$$\mathrm{Gr} = \frac{g\beta\,(T_w - T_\infty)\,L^3}{\nu^2}, \quad \mathrm{Pr} = \frac{\alpha}{\nu}, \quad \mathrm{Ra} = \mathrm{GrPr}\,. \tag{3}$$

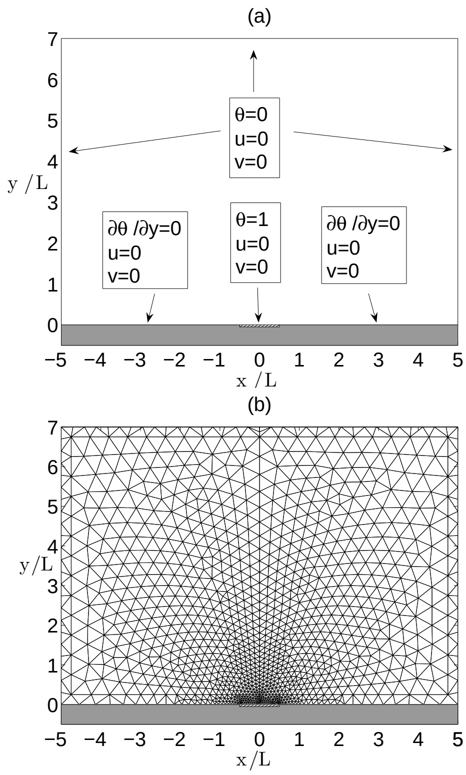

Figure 1. Schematic of the geometry, boundary conditions (a) and computational mesh (b). The spatial domain is composed of 2188 spectral elements each with 9×9 collocation points.

Figure 1 shows the computational domain and the boundary conditions which are very similar to those used by Martorell *et al.* [17]. Kimura *et al.* [14], Kimura *et al.* [15] and Martorell [17] *et al.* performed experiments with horizontal and inclined heated plates with imposed heat flux in similar domains. The flow starts from the rest.

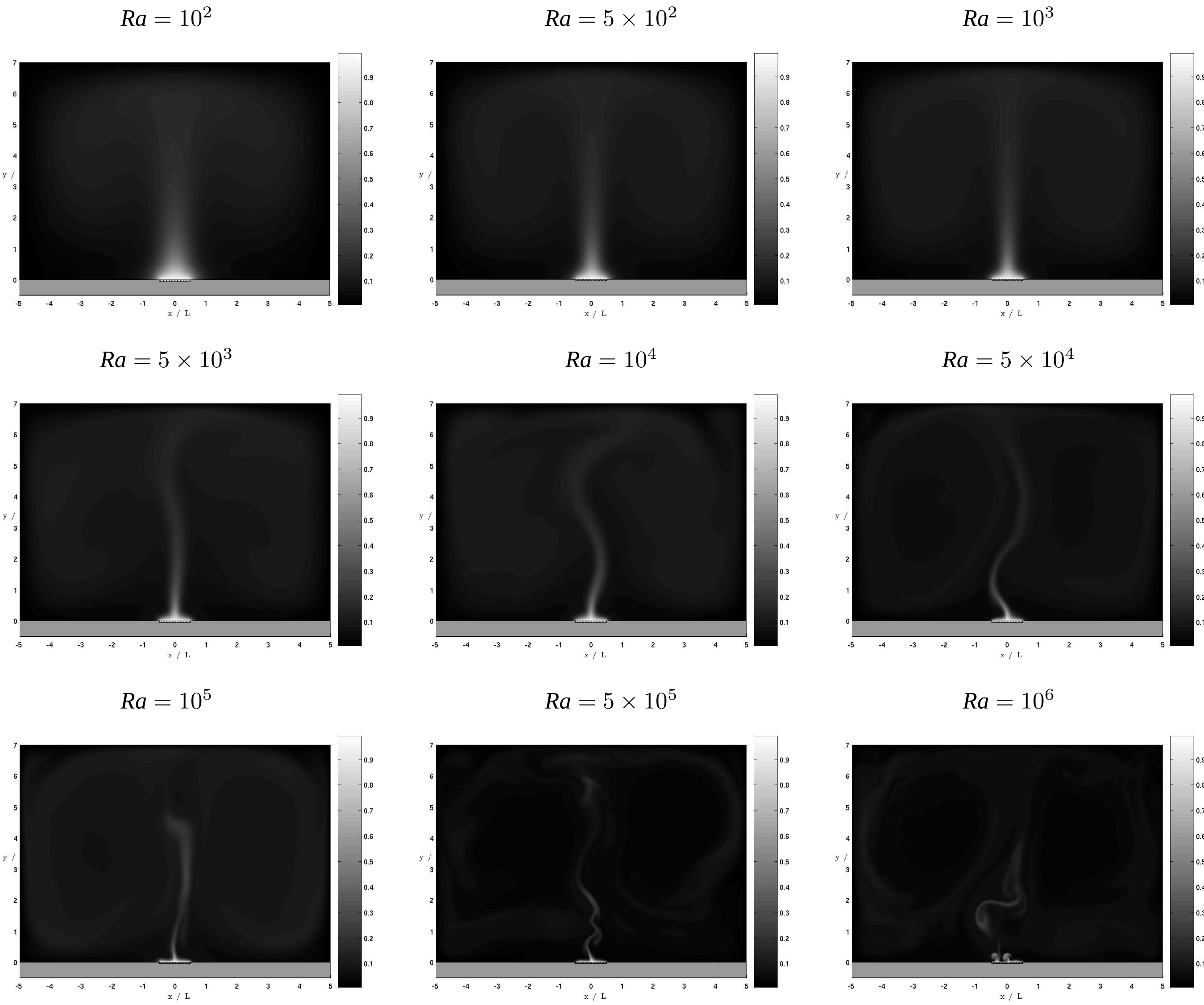

Figure 2. Dimensionless temperature field at different Rayleigh numbers.

Numerical results

Figure 2 shows some snapshots of the dimensionless temperature field at different Rayleigh numbers. Transition from steady to unsteady laminar convection is observed in the range $Ra = (2.5 \div 3.5) \times 10^3$. In figure 3 we plot the *local* Nusselt number at the plate surface

$$Nu\,(x^*, t^*) = \left(\frac{\partial \theta}{\partial y^*}\right)_{y=0} \qquad x^* \in [-0.5, 0.5] \tag{4}$$

for the snapshots shown in figure 2.

In order to compare the heat transfer's features of plates of various shapes Goldstein *et al* [9] proposed a length-scale L defined as the active surface divided by its perimeter. For our infinite horizontal strip we have

$$L = \lim_{b \to \infty} \frac{ab}{2\,(a+b)} = \frac{a}{2}\,, \tag{5}$$

where a denotes the width of the plate. Many experimental correlations $Nu - Ra$ such as those given by Al-Arabi & El-Riedy [2] and Bandrowskii & Rybski [5], originally based upon the width of the plate a, have been recalculated by Goldstein & Kei-Shun [8] as function of the area to perimeter length-scale L. In figure 4 we plot the correlations proposed in [2],[16],[5] and [9] for the dependence of the *averaged* Nusselt number on the Rayleigh number when these dimensionless groups are based on the area to perimeter ratio (see also [17]). Table 1 summarizes the aforementioned published experimental correlations and their range of applicability.

	c_1	c_2	Range of Ra_L
Goldstein *et al.* [9]	0.96	0.167	$1 \div 2 \times 10^2$
“ ”	0.59	0.25	$2 \times 10^2 \div 10^4$
Bandrowski *et al.* [5]	0.69	0.222	$3 \times 10^3 \div 2.5 \times 10^5$
Lloyd *et al.* [16]	0.54	0.25	$2 \times 10^4 \div 8 \times 10^6$
Al-Arabi *et al.* [2]	0.50	0.25	$2 \times 10^5 \div 8 \times 10^6$

Table 1. Experimental correlations $Nu_L = c_1 Ra_L^{c_2}$ for isothermal horizontal plates. The characteristic length is the active surface divided by its perimeter.

For time dependent natural convection (i.e. $Ra > 3.5 \times 10^3$)

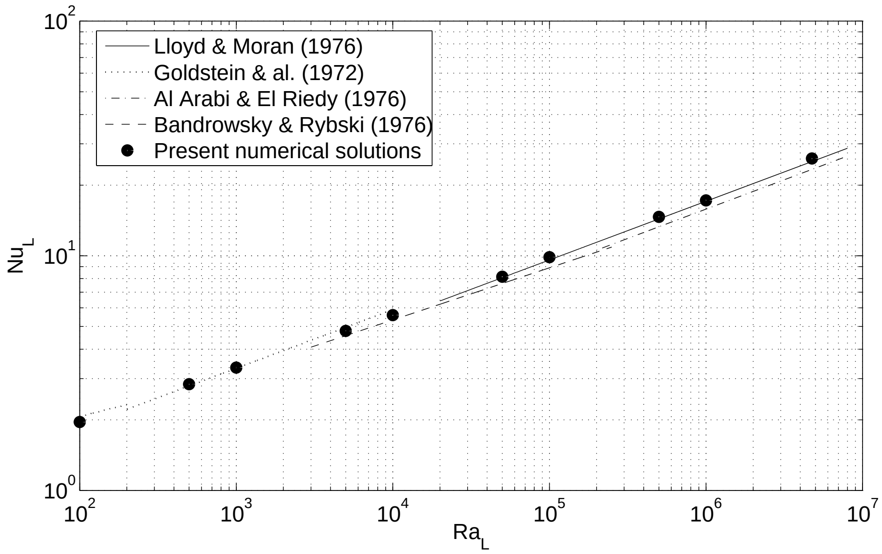

Figure 4. Published heat and mass transfer correlations for natural convection from horizontal plates. The area over perimeter ratio is used as characteristic length. Shown are also the results of our numerical simulations.

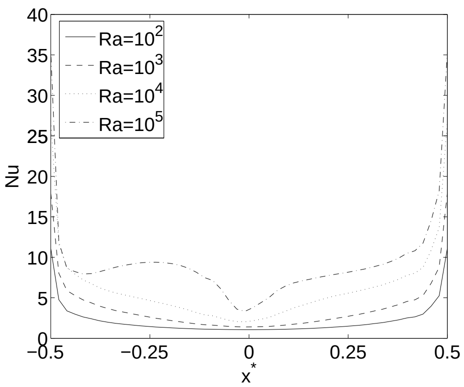

Figure 3. Local Nusselt number at the plate surface corresponding to the snapshots shown in figure 2.

Rayleigh number *Ra*	Averaged Nusselt number Nu_L
10^2	1.96
5×10^2	2.84
10^3	3.34
5×10^3	4.79
10^4	5.59
5×10^4	8.15
10^5	9.87
5×10^5	14.66
10^6	16.23
4.75×10^6	25.98

Table 2. Numerical results for the averaged Nusselt number.

we extracted 50 equidistant snapshots of the dimensionless temperature using a convenient sampling frequency in order to satisfy the Nyquist's criterion. The averaged Nusselt number

$$Nu_L = \frac{1}{t}\int_0^t \int_{-0.5}^{0.5} Nu\left(x^*, t^*\right) dx^* dt^* \,, \tag{6}$$

where t is period of observation, turns out to be in very good agreement with the experimental correlations (see figure 4). This supports the accuracy of the numerical scheme proposed in Appendix I. Table 2 summarizes the main findings for the averaged Nusselt number.

POD analysis of the temperature field at *Ra* $= 4.75 \times 10^6$

We consider the dimensionless flow at $Pr = 0.72$ and $Ra = 4.75 \times 10^6$, the latter being based upon the width of the plate a. This flow corresponds to the physical case of natural convection over an isothermal highly elongated plate of width $a = 0.1$ m at $T_w = 400$ K placed on an insulator of width 1 m inside a box of air of width 1 m and height 0.7 m with walls kept at $T_\infty = 300$ K. If we evaluate the physical properties of the air at the mean film temperature $T_f = (T_w + T_\infty)/2 = 350$ K we get $Pr = 0.719$ and $Gr \simeq 6.60 \times 10^6$, i.e. $Ra \simeq 4.75 \times 10^6$. A Fourier analysis of the time series for the velocity (figure 6) and the temperature fields reveals that the highest dimensionless time frequency is everywhere less than $f_{sup} = 6$. We extracted $S = 65$ regular spaced snapshots from the DNS using a dimensionless sampling frequency $f = 16 > 2f_{sup}$ in order to satisfy the Nyquist's criterion. The dimensionless frequency 0.246 characterizes the most energetic dimensionless vortex shedding close to the heated plate (see figure 6).

We investigate the dimensioneless tempertature field by the symmetric version of the proper orthogonal decomposition method [4; 3]. Essentially this consists in representing the dimensioneless temperature by a *biorthogonal* series

$$\theta(\mathbf{x}, t) = \sum_{k=1}^{\infty} \sqrt{\mu_k}\,\Phi_k(\mathbf{x})\,\psi_k(t) \tag{7}$$

where the functions ψ_k and Φ_k are the solutions of the following

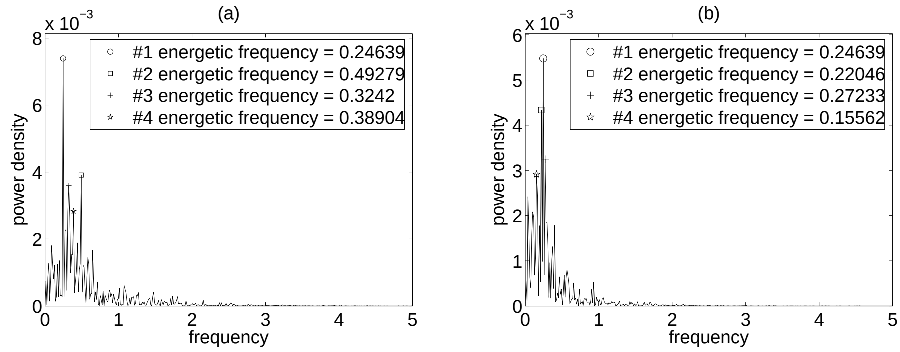

Figure 6. Fourier spectrum of the time series for the y (a) and x (b) velocity components at the point $x^* = -0.1, y^* = 0.23$.

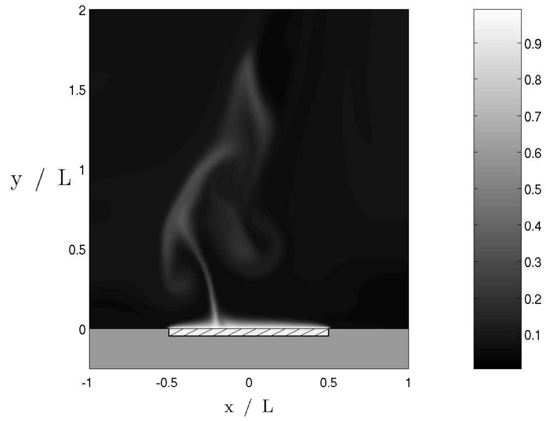

Figure 5. Dimensionless temperature field at *Ra* $= 4.75 \times 10^6$.

eigenvalue problems

$$\left(\Theta^\dagger \Theta \Phi_k\right)(\mathbf{x}) = \int_\Omega \mathcal{S}\left(\mathbf{x}, \mathbf{x}'\right) \Phi_k\left(\mathbf{x}'\right) d\mathbf{x}' = \mu_k \Phi_k\left(\mathbf{x}\right) \ , \quad (8)$$

$$\left(\Theta \Theta^\dagger \psi_k\right)(t) = \int_T \mathcal{T}\left(t, t'\right) \psi_k\left(t'\right) dt' = \mu_k \psi_k\left(t\right) \ . \quad (9)$$

In (8)-(9) $\mathcal{S}\left(\mathbf{x}, \mathbf{x}'\right)$ and $\mathcal{T}\left(t, t'\right)$ are the spatial and the temporal autocorrelations of the temperature field defined by

$$\mathcal{S}\left(\mathbf{x}, \mathbf{x}'\right) = \int_T \theta\left(\mathbf{x}, t\right) \cdot \theta\left(\mathbf{x}', t\right) dt \, , \quad (10)$$

$$\mathcal{T}\left(t, t'\right) = \int_\Omega \theta\left(\mathbf{x}, t\right) \cdot \theta\left(\mathbf{x}, t'\right) d\mathbf{x} \, . \quad (11)$$

The POD modes ψ_k and Φ_k are not independent as there exist a one-to-one correspondence between them in the form

$$\left(\Theta \Phi_k\right)(t) \equiv \int_\Omega \theta\left(\mathbf{x}, t\right) \cdot \Phi_k\left(\mathbf{x}\right) d\mathbf{x} = \sqrt{\mu_k} \psi_k\left(t\right) \ , \quad (12)$$

$$\left(\Theta^\dagger \psi_k\right)(\mathbf{x}) \equiv \int_T \theta\left(\mathbf{x}, t\right) \psi_k\left(t\right) dt = \sqrt{\mu_k} \Phi_k\left(\mathbf{x}\right) \ . \quad (13)$$

These relations, called *dispersion* relations (see [4],[3]), characterize the link between the spatial and the temporal evolution of the system. The POD analysis of the temperature field at *Ra* $= 4.75 \times 10^6$ is shown in figure 7. The first temperature mode represents the time averaged temperature which carries on the 96% of the total energy (see figure 7(a)). This justifies the steady state numerical (or analytical) solutions for natural convection above horizontal plates and the usage of low frequency acquisition systems to measure the Nusselt number. The time averaged (or *mean*) heat flux at the plate surface can be written as

$$\left\langle q \right\rangle_t = \frac{\kappa\left(T_w - T_\infty\right)}{L} \left(\frac{\partial \left\langle \theta \right\rangle_t}{\partial y^*}\right)_{y=0} \quad (14)$$

$$= \frac{\mu_1 \kappa\left(T_w - T_\infty\right)}{L\sqrt{t}} \left(\frac{\partial \Phi_1}{\partial y^*}\right)_{y=0} \quad (15)$$

(see figure 7(b)) where κ is the thermal conductivity of the fluid and $\left\langle \cdot \right\rangle_t = \frac{1}{t}\int_t (\cdot) dt'$ is the averaging operator. Let us approximate the heat flux at the plate surface by a third order temperature POD expansion

$$q \simeq \left\langle q \right\rangle_t + \frac{\kappa\left(T_w - T_\infty\right)}{L} \left(\mu_2 \psi_2 \left(\frac{t}{\tau}\right) \left.\frac{\partial \Phi_2}{\partial y^*}\right|_{y=0} + \right. \quad (16)$$

$$\left. + \mu_3 \psi_3 \left(\frac{t}{\tau}\right) \left.\frac{\partial \Phi_3}{\partial y^*}\right|_{y=0} \right) \quad (17)$$

where τ is the time scale. From the structure of the second and the third temperature POD modes shown in figure 7(c)(d) (spatial modes) and figure 8 (temporal modes) respectively, we can draw conclusions on the main mechanism responsible for the heat transfer. In fact the symmetric-like structure of Φ_2 and Φ_3 and the periodic-like behavior of the corresponding temporal modes (figure 8) implies that the heat flux at the plate surface is waveform-like in time and symmetric in space, 0.246 being the main dimensionless time frequency for both the aforementioned temperature modes. Such frequency is in very good agreement with the main vortex shedding time frequency. This supports the conclusion that this temperature coherent structure is determined by advection. Therefore the most energetic temporal evolution of the chaotic heat transfer is characterized by the source zones highlighted in figure 7(c)-(d) moving on the plate surface symmetrically and periodically from the center to the plate edges.

Summary

We performed direct numerical simulations of natural convective flows over isothermal horizontal plates in confined domains. We investigated a wide range of Rayleigh numbers from

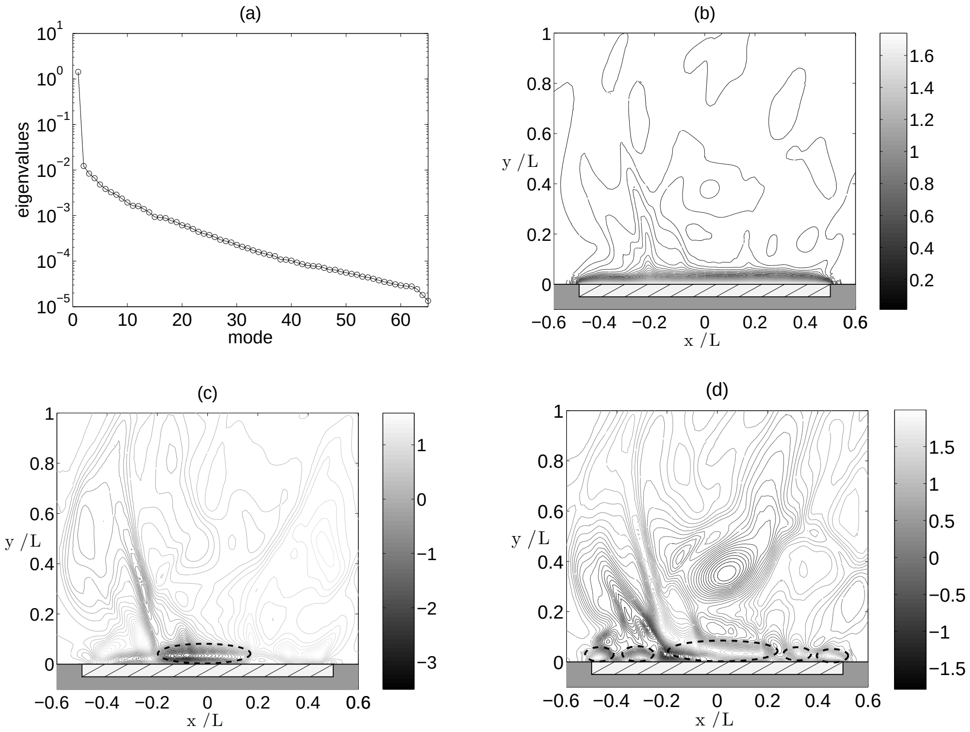

Figure 7. POD eigenspectrum (a) and isocontours of the first three temperature spatial POD modes Φ_1 (b), Φ_2 (c) and Φ_3 (d).

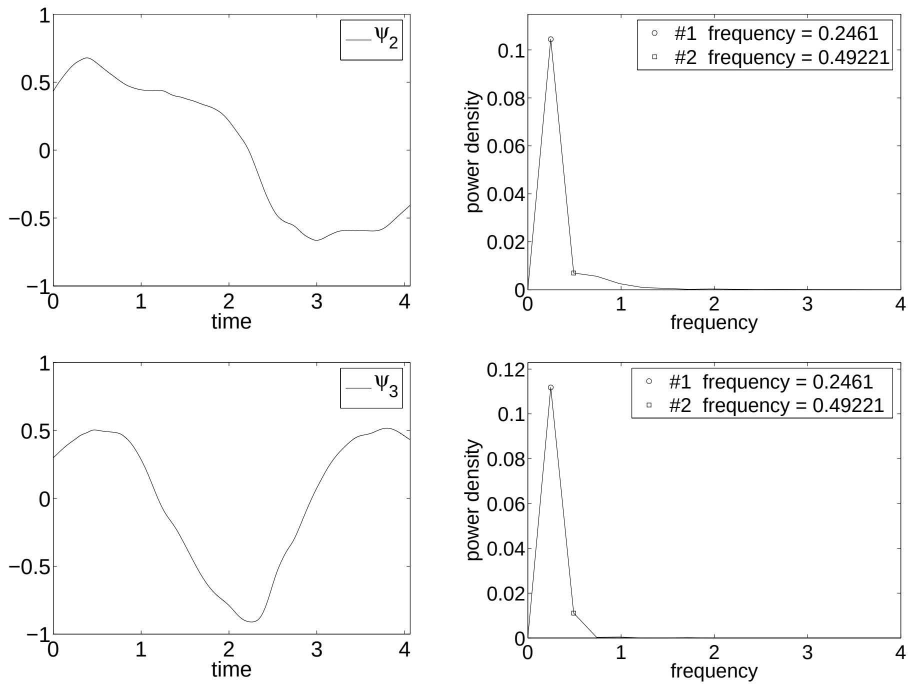

Figure 8. Temporal POD modes ψ_2 and ψ_3 and their Fourier analysis.

$Ra = 10^2$ to $Ra = 4.75 \times 10^6$. Transition form steady to unsteady state is observed in the interval $Ra = (2.5 \div 3.5) \times 10^3$. The computed correlation between the averaged Nusselt number and the Rayleigh number turns out to be in very good agreement with the experimental correlations. The proper orthogonal decompostion of the temperature field at Rayleigh number $Ra = 4.75 \times 10^6$ reveals the existence of organized spatio-temporal structures which characterize the evolution of the main heat transfer's features at the plate surface.

APPENDIX I

Basic details of the numerical scheme

To discretize the equations (1) we use the high order splitting scheme described in [11] both for Fourier and Navier-Stokes equations. The splitting scheme, involves the following substeps:

$$\widehat{\theta} = \sum_{q=0}^{J_i-1} \alpha_q \theta^{n-q} + \Delta t \sum_{q=0}^{J_e-1} \beta_q \left[\mathbf{u} \cdot \nabla \theta\right]^{n-q} \qquad (18)$$

$$\left(\nabla^2 - \frac{\gamma_0 \mathrm{RePr}}{\Delta t}\right)\theta^{n+1} = -\frac{\mathrm{RePr}}{\Delta t}\widehat{\theta} \tag{19}$$

$$\widehat{\mathbf{u}} = \sum_{q=0}^{J_i-1}\alpha_q \mathbf{u}^{n-q} + \Delta t\left[\sum_{q=0}^{J_e-1}\beta_q\left([(\mathbf{u}\cdot\nabla)\,\mathbf{u}]^{n-q} + \mathbf{j}\frac{\mathrm{Gr}}{\mathrm{Re}^2}\theta^{n-q+1}\right)\right] \tag{20}$$

$$\nabla p^{n+\frac{1}{2}} = \nabla\cdot\left(\frac{\widehat{\mathbf{u}}}{\Delta t}\right) \tag{21}$$

$$\left(\nabla^2 - \frac{\gamma_0 \mathrm{Re}}{\Delta t}\right)\mathbf{u}^{n+1} = -\frac{\mathrm{Re}}{\Delta t}\widehat{\mathbf{u}} - \mathrm{Re}\nabla p^{n+\frac{1}{2}} \tag{22}$$

where J_e and J_i are the order of integration (we use $J_e = J_i = 3$) for the advection and the diffusion terms respectively (stiffly stable SE/SI scheme [11]). For the spatial discretization we use an 8^{th} order spectral finite element method (see [11] and [12]). Also, $\mathbf{u}^{n+1}$ denotes the velocity field at the iteration $n+1$. As usual in the spectral projection method, the divergence free constraint for the velocity field is enforced in the fourth sub-step, i.e. equation (21).

NOMENCLATURE

a Width of the plate
Gr Grashof Number
κ Fluid thermal conductivity
L Area to perimeter length scale
Nu Local Nusselt number
Nu_L Averaged Nusselt number
p Dimensionless piezometric pressure
Pr Prandtl Number
q Heat flux at the plate surface
Ra Rayleigh Number
Re Reynolds Number
$\mathcal{S}$ Spatial autocorrelation
t Dimensionless period of observation
$\mathcal{T}$ Temporal autocorrelation
$\mathbf{u}$ Dimensionless velocity field
x^* Dimensionless horizontal coordinate
y^* Dimensionless vertical coordinate

Greek symbols

α_q Coefficients for Adams-Bashforth integration scheme
β_q Coefficients for Adams-Bashforth integration scheme
Φ_k POD spatial modes
μ_k POD eigenvalues (energy)
ψ_k POD temporal modes
θ Dimensionless temperature field
Θ Integral operator with kernel θ
$\Theta^\dagger$ Adjoint of Θ
τ Time scale

REFERENCES

[1] GJESDAL, T., WASBERG, C. & ANDREASSEN, O. 2003 Spectral element simulations of buoyancy-driven flow. *Second National Conference on Computational Mechanics, Trondheim* .

[2] AL-ARABI, M. & EL-RIEDY, M. 1976 Natural convection heat transfer from isothermal horizontal plates of different shapes. *Int. J. Heat Mass Transfer* **19**, 1399–1404.

[3] AUBRY, N. 1991 On the hidden beauty of the proper orthogonal decomposition. *Theoret. Comput. Fluid Dynamics* **2**, 339–352.

[4] AUBRY, N., GUYONNET, N. & LIMA, R. 1991 Spatio-temporal analysis of complex signals: theory and applications. *J. Statistical Physics* **64**, 683–739.

[5] BANDROWSKI & RYBSKI, W. 1976 Free convection mass transfer from horizontal plates. *Int.J.Heat Transfer* **19**, 827.

[6] CHAMBERS, B. & LEE, T. 1997 A numerical study of local and average natural convection Nusselt numbers for simultaneous convection above and below a uniformly heated horizontal thin plate. *J. Heat Transfer* **119**, 102–108.

[7] FUJII, T. & IMURA, H. 1972 Natural convection heat transfer from a plate with arbitrary inclination. *Int. J. Heat Mass Transfer* **15**, 755–767.

[8] GOLDSTEIN, R. & KEI-SHUN, L. 1983 Laminar natural convection from a horizontal plate and the influence of plate edge extensions. *J. Fluid Mech.* **129**, 55–75.

[9] GOLDSTEIN, R., SPARROW, E. & JONES, D. 1973 Natural convection mass transfer adjacent to horizontal plates. *Int. J. Heat Mass Transfer* **16**, 1025–1035.

[10] HASSAN, K. & MOHAMED, S. 1970 Natural convection from isothermal flat surfaces. *Int. J. Heat Mass Transfer* **13**, 1873–1886.

[11] KARNIADAKIS, G. & SHERWIN, S. 1999 *Spectral/hp element methods for CFD*. Oxford Univ. Press.

[12] WARBURTON, T. 1999 Spectral/hp methods on polymorphic multi-domains: algorithms and applications. PhD thesis, Brown University.

[13] BADE, F. & HALDENWALG, P. 1998 High order scheme for thermally driven flow in an open channel. *Computer and Fluids* **27** (2), 273–290.

[14] KIMURA, F., YOSHIOKA, T., KITAMURA, K., YAMAGUCHI, M. & ASAMI, T. 2002 Fluid flow and heat transfer of natural convection at slightly inclined, upward-facing, heated plate. *Heat Transfer-Asian Research* **35** (5), 362–375.

[15] KITAMURA, K. & KIMURA, F. 1995 Heat transfer and fluid flow of natural convection adjacent to upward-facing horizontal plates. *Int. J. Heat Mass Transfer* **38**, 3149–3159.

[16] LLOYD, J. & MORAN, W. 1974 Natural convection adjacent to horizontal surface of various platforms. *Int. J. Heat Mass Transfer* **96**, 443–447.

[17] MARTORELL, I., HERRERO, J. & GRAU, F. 2003 Natural convection from narrow horizontal plates at moderate rayleigh numbers. *Int. J. Heat Mass Transfer* **46**, 2389–2402.

[18] SPARROW, E. & CARLSON, C. 1986 Local and average natural convection Nusselt numbers for a uniformly heated, shrouded or unshrouded horizontal plate. *Int. J. Heat Mass Transfer* **29**, 369–379.

[19] YOUSEF, W., TARASUK, J. & MCKENN, W. 1982 Free convection heat transfer from upward-facing isothermal horizontal surfaces. *J. Heat Transfer* **104**, 493–500.